Voltage Difference-Based Field-Weakening Control of Double-Rotor Hybrid Excitation Axial Flux Switching Permanent Magnet Motor

M. Kamali*, B. Rezaeealam*(C.A.) and F. Rezaee-Alam *

Abstract: This paper investigates the operational performance of a novel Double-Rotor Hybrid Excitation Axial Flux Switching Permanent Magnet (DRHE-AFSPM) machine, combining the strengths of Flux-Switching Machines and Hybrid Excitation Synchronous Machines. The study analyzes the machine's structure and magnetic field adjustment principles, including inductance and flux linkage characteristics. A mathematical model is derived and a vector control-based drive system is established. The loading capacity of the DRHE-AFSPM motor is examined at low speeds using an $i_d = 0$ control approach based on a stage control strategy. For high-speed operation, a field-weakening control strategy is implemented, with the field-weakening moment determined based on the voltage difference. Simulations and experimental results demonstrate the DRHE-AFSPM motor's ability to fully utilize its torque with $i_d = 0$ control, highlighting its strong load capacity. Compared to speed-based field-weakening control strategies, the voltage difference-based approach offers improved inverter output voltage utilization and a broader speed regulation range. These findings suggest that the DRHE-AFSPM motor is a promising candidate for in-wheel motor applications in electric vehicles (EVs).

Keywords: Axial Flux, Hybrid Excitation, Field-weakening control, PM

1 Introduction

THE growing depletion of fossil fuels and the escalating environmental pollution have spurred rapid development in the field of EVs. EV drive systems are characterized by their high starting torque and wide constant power operating range. While various electric motors are employed in EVs, including induction motors, switched reluctance motors, and permanent magnet synchronous motors (PMSMs), PMSMs have gained widespread adoption due to their simple structure, high power density, and high efficiency. However, the inherent difficulty in regulating the air gap

magnetic field presents limitations for PMSMs. To broaden the constant power operating range, a common approach is to utilize negative d-axis current for field weakening. However, excessive weakening can lead to permanent magnet demagnetization. This pursuit of high-power density, high efficiency, and wide speed operating range in EV drive systems has driven the development of hybrid excitation motors, which emphasize magnetic capability [1]. These motors offer a promising solution to overcome the limitations of traditional PMSMs and enhance the performance of EV drive systems.

The Double-Rotor Hybrid Excitation Axial Flux Switching Permanent Magnet (DRHE-AFSPM) machine represents a novel design that effectively combines the strengths of permanent magnet synchronous motors (PMSMs) and electrically excited synchronous motors, overcoming the limitations of each individual technology. This innovative approach results in a motor with a high-power factor and a wide speed operating

range. The DRHE-AFSPM machine utilizes two distinct excitation sources: permanent magnet excitation and electric excitation. These sources interact within the air gap of the motor, generating a combined air gap magnetic field. When the electric excitation coil carries a forward excitation current, it produces a magnetic flux that aligns with the permanent magnet flux, leading to an enhanced air gap magnetic field. This magnetization enhancement operation provides high torque, ideal for starting or climbing in EVs. Conversely, when the electric excitation coil carries a reverse excitation current, it generates a magnetic flux that opposes the permanent magnet flux, resulting in a weakened air gap magnetic field. This field weakening capability significantly expands the motor's constant power operation range, effectively meeting the requirements of high-speed cruising in EVs. This unique design concept, explored in various studies [2-6], offers a compelling solution for enhancing the performance and versatility of EV drive systems.

In [7], a sophisticated torque control technique was introduced for a high saliency ratio permanent magnet (PM) motor. This method aims to achieve independent control of currents to ensure smooth torque under varying speed and load conditions by leveraging the stator magnetic flux and current of the motor. However, accurately estimating the electromagnetic torque and stator magnetic flux poses a challenge due to motor parameter variations, which can result in reduced system control accuracy. To enhance parameter estimation precision, a refined torque control method based on voltage distribution state filters was proposed in [8]. This method effectively mitigates torque fluctuations during magnetization state adjustments, thereby minimizing the impact of parameter variations on control accuracy and bolstering the resilience of electromagnetic torque control.

Induction potential measurement techniques encompass voltage sensor methods and magnetic flux observer methods. Due to cost constraints, voltage sensor methods are typically not employed in drive control systems. In scenarios where the motor operates at low or zero speeds, the induction potential is minimal, making it challenging for the magnetic flux observer method to accurately monitor the motor's PM flux. To tackle this issue, a magnetization state adjustment method based on high-frequency signal injection was introduced. This method entails applying high-frequency voltage signals to the armature windings and analyzing the resulting high-frequency current response to ascertain the motor's magnetization state. By adjusting the magnetization state based on this information, the motor's performance across diverse operating conditions can be optimized.

Nevertheless, fluctuations in the observed PM flux during the magnetization state adjustment process can lead to frequent adjustments, as highlighted in [9] and [10]. In the high-speed range, these adjustments may even pose a risk of damaging the inverter power components. To address this concern, a magnetization state adjustment method employing a hysteresis controller was proposed. By examining the electromagnetic torque and speed characteristics of the motor under various conditions, researchers were able to evaluate the motor's efficiency under different magnetization states. Additionally, to mitigate steady-state errors associated with the hysteresis controller, an integral compensation-based magnetization state adjuster was introduced.

In [11], a novel maximum torque current ratio control method coupled with magnetization state adjustment for a PM motor was introduced. The motor's nonlinear inductance characteristics and adjustable PM magnetization state posed challenges for conventional control methods. Leveraging the data fitting capabilities of artificial neural networks, researchers proposed a maximum torque control method based on artificial neural networks. This innovative approach enables precise real-time adjustment of direct and quadrature axis currents, thereby enhancing motor efficiency and torque capabilities.

For rotor PM control, a method was proposed in [12]. During regular motor operation, $i_d=0$ control is employed; however, in instances where online magnetization state adjustment is necessary, a feedforward voltage control method based on the inverse motor model is applied to the direct axis component, while the quadrature axis component utilizes current feedback control. Once the online magnetization state adjustment is completed, the control reverts back to $i_d=0$. Notably, the motor exhibits angular dependence during the magnetization state adjustment process, necessitating the application of two pulse currents at the same position to adjust the magnetization state of all permanent magnets.

While field-weakening control strategies outlined in [13-16] rely on speed-based judgment of the field-weakening moment, they suffer from a significant limitation: incomplete utilization of the inverter output voltage. This shortcoming is addressed in [17] by introducing the concept of a field-weakening base speed. The motor enters a field-weakening state when its operating speed exceeds this base speed. However, the calculation of the field-weakening base speed proves to be a complex and error-prone process. This analysis highlights a key challenge in existing field-weakening control strategies. The reliance on speed-based judgment and the intricate calculation of the base speed hinder the

optimal utilization of the inverter's potential.

In general, despite the advancements in control strategies, several significant limitations need to be addressed. Firstly, field-weakening techniques rely on speed-based judgments for determining the field-weakening moment, which can lead to undesirable accidental demagnetization. This phenomenon often arises from the q-axis armature reaction, which affects system stability and performance. Secondly, the complexity inherent in drive control and the manipulation of the magnetization state presents a considerable challenge, complicating the implementation and operational management of the system. Furthermore, there are strict limitations on the power rating permitted for the magnetization state manipulation pulse, which restricts the potential of the system to deliver optimal torque and efficiency during various operating conditions. Lastly, the effectiveness of magnetization state manipulation exhibits a strong angular dependence, resulting in inconsistent performance across different positions and speeds. These combined challenges highlight the need for further research to develop more robust and efficient field-weakening control strategies that overcome these limitations.

This paper introduces a novel double-rotor hybrid excitation axial field flux-switching PM (DRHE-AFSPM) motor, combining the advantages of flux-switching technology and hybrid excited synchronous machines (HESM). The DRHE-AFSPM motor features a unique topology with all windings, permanent magnets, and excitation windings located on the stator. This configuration significantly shortens the main magnetic circuit, leading to higher air gap magnetic density with reduced PM material usage. Consequently, the motor achieves a smaller volume, higher torque density. The hybrid excitation method enables stronger weak magnetic acceleration capabilities and a wider operating speed range. Additionally, the simplified rotor design, devoid of windings and permanent magnets, contributes to a simple, reliable, and easily cooled structure. While the complexity of the DRHE-AFSPM machine structure and control leads to a higher price compared to conventional PM synchronous motors, the motor offers high operating efficiency over a wide speed range, particularly in the high-speed region. This makes the DRHE-AFSPM motor suitable for applications requiring wide-speed range and variable speed drive operation, such as EVs. The organization of this paper is as follows: section II introduces the DRHE-AFSPM topology and outlines the mechanisms for magnetic field regulation. Section III establishes the mathematical model based on the rotor reference frame. In Section IV, a partition control strategy is implemented, featuring an i_d=0 control approach for the low-speed region and a field-weakening control strategy for the high-speed region. This field-weakening strategy utilizes voltage difference judgments of the weak magnetic moment to enhance operational efficiency. Finally, Section V presents the development of the control system model for the DRHE-AFSPM, along with simulation and experimental research conducted using MATLAB/Simulink and dSPACE1103. The results validate the effectiveness of the proposed control strategy.

2 DRHE-AFSPM Topology and Magnetic Field Regulation Mechanism

2.1 Topology

The paper investigates a 3-phase 6/11 pole hybrid permanent magnet axial field flux-switching motor [18] (DRHE-ASFPM), which is depicted in Figure 1. This motor configuration comprises two identical external rotors and an internal stator, effectively representing the parallel connection of two single air gap axial flux motors. The stator design features a back-to-back arrangement, incorporating 6 H-shaped silicon steel sheet unit cores, as illustrated in Figure 1(b), along with 6 radially magnetized permanent magnets, 12 concentrated armature windings, and 12 concentrated excitation windings. The permanent magnets are positioned between the two H-shaped cores, while the excitation windings, responsible for magnetization or demagnetization, are wound around the middle teeth of the H-shaped cores. This configuration ensures effective magnetic isolation between phases, enhancing fault tolerance capabilities. By enabling the back-to-back connection of armature windings or excitation windings in series or parallel, the motor offers enhanced control flexibility. With the permanent magnets and windings housed in the stator, the rotor structure is characterized by its simplicity and robustness, making the motor particularly well-suited for EV drive systems. The design of the DRHE-ASFPM motor not only optimizes performance but also prioritizes reliability and ease of maintenance, aligning with the demanding requirements of EV applications.
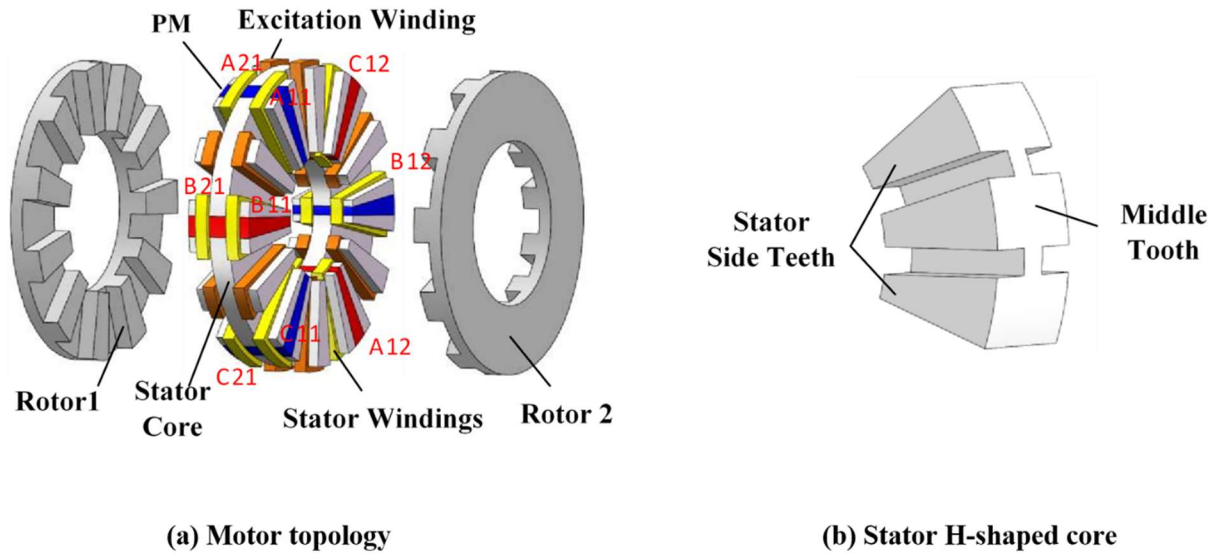
(a) Motor topology

(b) Stator H-shaped core

Fig. 1. Topology of DRHE-ASFPM machine

2.2 Magnetic Field Regulation Mechanism

The analysis and validation of the magnetic field adjustment principles of the DRHE-ASFPM motor have been conducted using a 3-D finite element method (FEM), as depicted in Figure 2. In the illustration, the black arrow lines denote the path of the PM flux, while the red arrow lines represent the excitation flux path. Notably, the PM flux and the excitation flux operate in parallel within the motor's magnetic circuit.

In the absence of excitation winding current, no excitation flux is produced, and the air gap field is solely generated through the interaction between the PM and the armature winding. This scenario corresponds to the PM excitation mode of the DRHE-ASFPM motor, akin to a dual rotor axial flux switching PM motor. As the rotor transitions from position 1 to position 2, the PM flux linkage in the armature winding fluctuates periodically, facilitating axial flux switching.

Upon energizing the excitation winding with positive current, the excitation flux linkage aligns with the PM flux linkage, bolstering the air gap field and enabling magnetization operation. This enhancement leads to increase of torque, particularly beneficial for providing high torque for EV starting or climbing. Conversely, applying negative current to the excitation winding causes the excitation flux linkage to oppose the PM flux linkage, weakening the air gap field, expanding the constant power operation range, and meeting the demands of high-speed cruising for EVs.

In cases of armature winding faults, such as open-circuiting or short-circuiting, or irreversible demagnetization of the permanent magnet, adjusting the excitation current allows for the reconstruction of the air gap field. This adjustment not only enhances torque but also reduces torque ripple, enabling fault-tolerant operation under faulty conditions and enhancing overall system reliability. Figure 2 illustrates that the excitation current-generated magnetic flux and the permanent magnet-generated magnetic flux in the DRHE-ASFPM motor are arranged in a parallel configuration within the magnetic circuit. This design surpasses the limitations of series magnetic potential hybrid excitation motors, offering independent control over both flux paths and providing greater flexibility in magnetic field manipulation. In summary, comprehensive examination of the DRHE-ASFPM motor's magnetic field control mechanisms highlights its potential for high-performance applications, particularly in EV propulsion systems. The motor's ability to finely adjust the magnetic field allows for a wide speed range of operation, improved torque characteristics, and enhanced reliability across various operating conditions.

3 Inductance Characteristics and Mathematical Model of DRHE-AFSPM machine

3.1 Inductance Characteristics

Inductance plays a crucial role in the performance of DRHE-AFSPM machines, impacting various aspects such as external characteristics, electromagnetic torque, and dynamic and static behaviors. The interaction between the excitation current's magnetic field, armature current, and the permanent magnet's magnetic field leads to a complex three-dimensional distribution of magnetic fields within the motor. To accurately study the inductance properties of DRHE-AFSPM machines, a three-dimensional finite element model was developed

and analyzed. The obtained inductance characteristics are depicted in Figure 3, showcasing the self-inductance and mutual inductance of the armature winding in Figures 3(a) and (b). These inductance values exhibit three-phase symmetry with a high degree of sinusoidality. Figure 3(c) illustrates the mutual inductance between the single-phase excitation winding and the armature winding, revealing its dependence on the rotor position. The mutual inductance curve follows a sinusoidal pattern within one electrical cycle.

Additionally, Figure 3(d) presents the self-inductance of the excitation winding in both field-enhancing and field-weakening modes of operation. Interestingly, the self-inductance of the excitation winding remains relatively constant throughout the rotor's position changes, regardless of whether the winding is supplied with a field-enhancing or field-weakening current. This constancy indicates a consistent self-inductance value under different operating conditions.
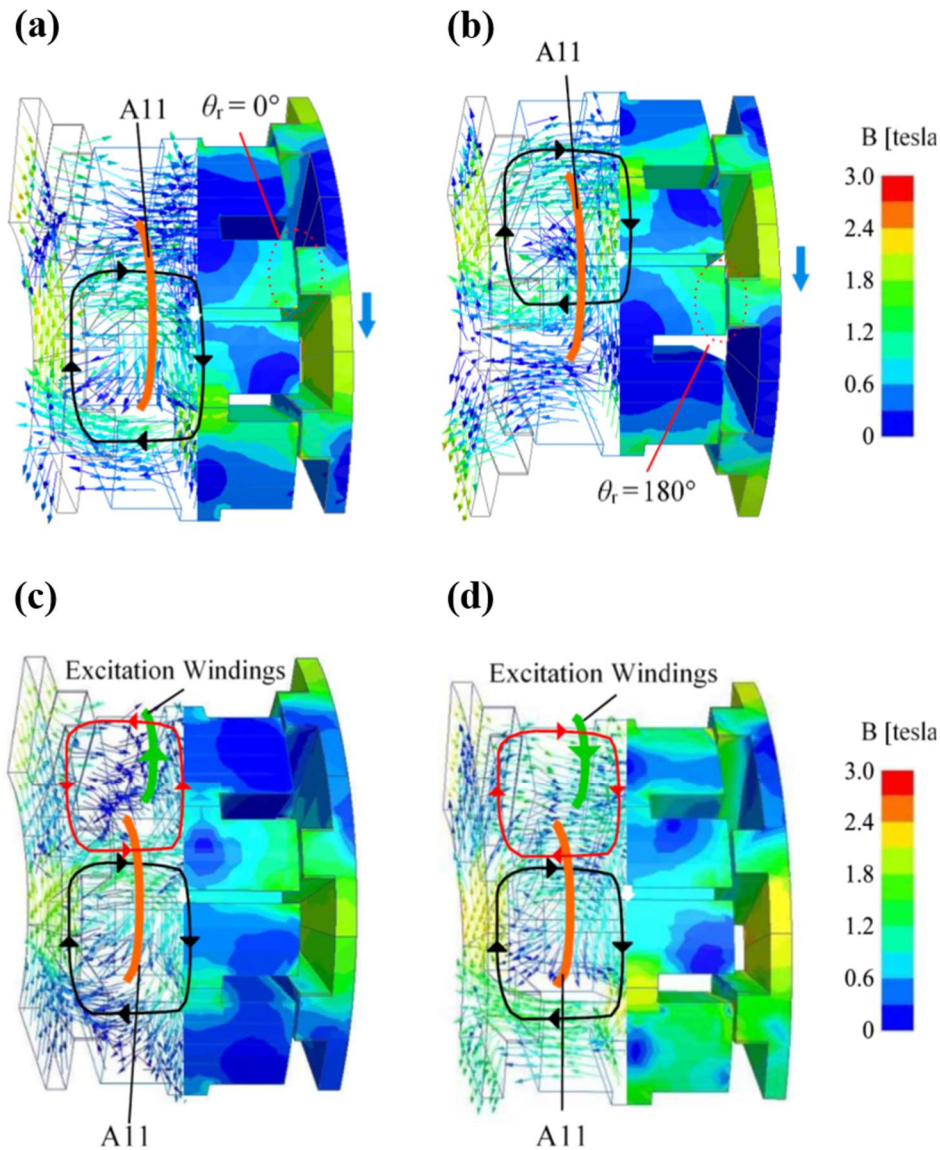

Fig. 2. Adjustment principles of magnetic field for DRHE-AFSPM machine (a) Position 1. (b) Position 2 (c) Field-enhancing (d) Field-weakening.
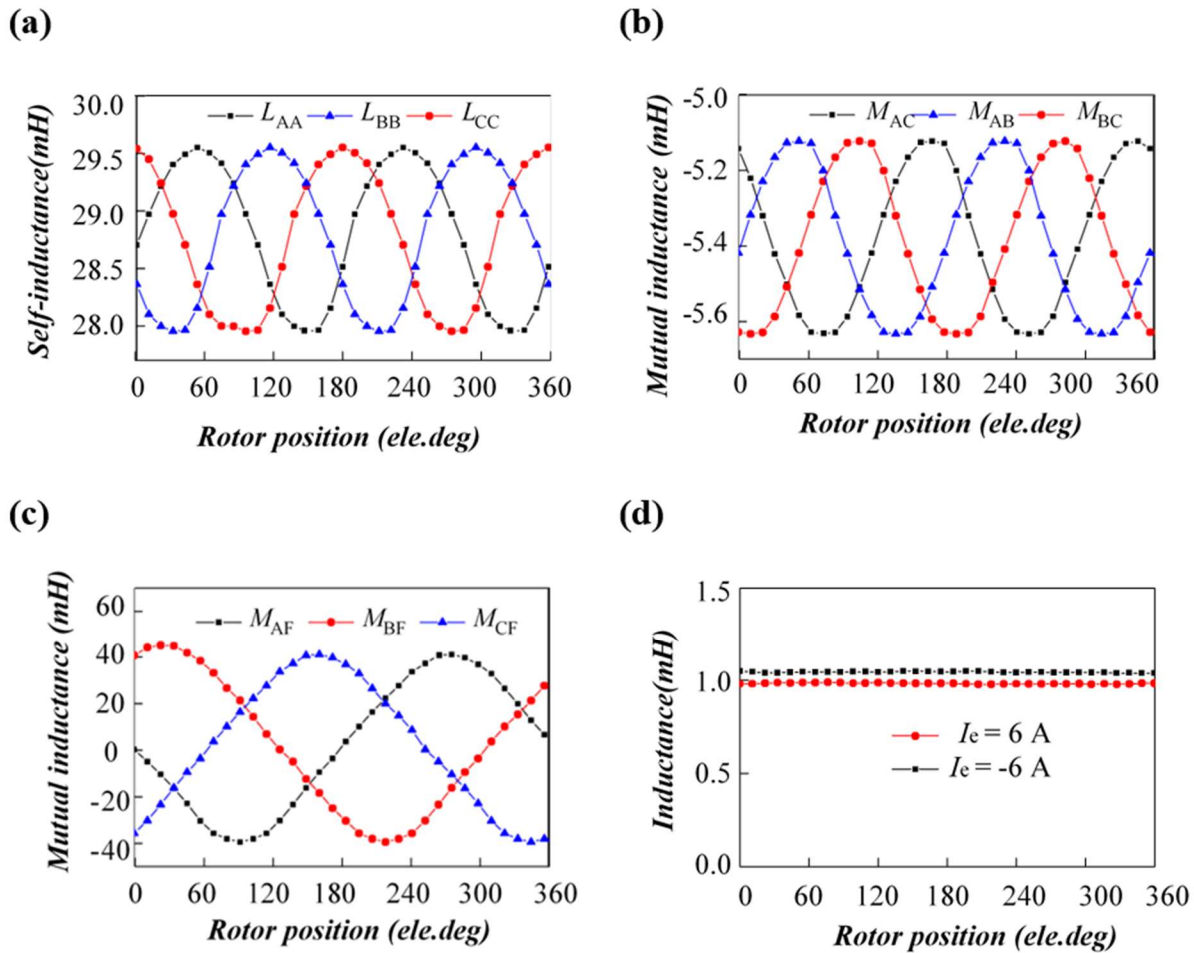
(a)

(b)

(c)

(d)

Fig. 3. Inductance characteristics of DRHE-AFSPM motor. (a) self-inductance of the armature winding (b) mutual inductance of the armature winding (c) mutual inductance between the excitation winding and the armature winding (d) self-inductance of the excitation winding.
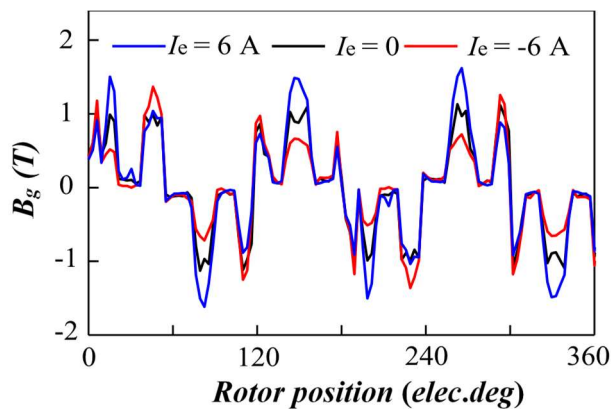

Fig. 4. The air gap magnetic flux density at the average radius

Using the 3-D FEM, the waveform of the air gap magnetic flux density at the average radius is calculated for three different operating modes: permanent magnet, field enhancing, and field weakening modes. As shown in Figure 4, when a positive excitation current is applied, the air gap magnetic flux density increases at the teeth positions on the stator side and decreases at the teeth positions in the middle of the stator. In the field weakening mode, the characteristics of the air gap magnetic flux density variation are opposite.

3.2 Inductance Characteristics

As mentioned earlier, the DRHE-AFSPM motor demonstrates a sinusoidal distribution of magnetic flux and inductance, similar to the rotor-type hybrid excitation PM (HEPM) motor. It is assumed that the permanent magnets and the DC excitation coil on the stator of the DRHE-AFSPM are positioned on the rotor, considering temperature, magnetic saturation, and hysteresis losses being disregarded. The analysis of the DRHE-AFSPM motor is conducted using the rotor magnetic field-oriented d-q coordinate system, and its equivalent model is illustrated in Figure 5.
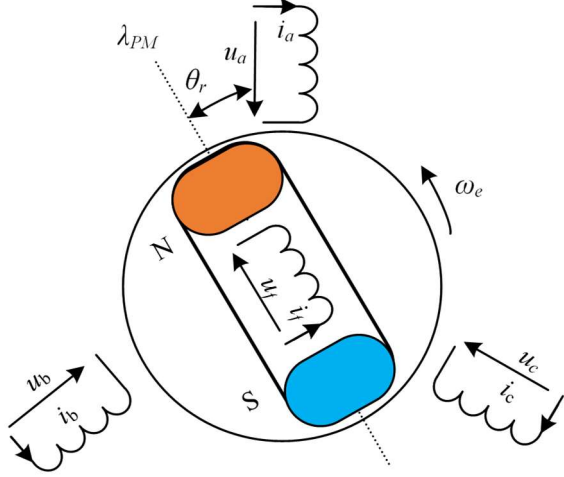
Fig. 5. DRHE-AFSPM motor in *d-q* reference frame

From the equivalent model shown in Figure 5, the magnetic flux equations and voltage equation of DRHE-AFSPM motor in the *d-q* coordinate system are derived as follows:

$$\begin{cases} u_d = R_s i_d + \dfrac{d\lambda_d}{dt} - \omega_e \lambda_q \\[2mm] u_q = R_s i_q + \dfrac{d\lambda_q}{dt} + \omega_e \lambda_d \\[2mm] u_f = R_f i_f + \dfrac{d\lambda_f}{dt} \\[2mm] \lambda_d = L_d i_d + M_{sf} i_f + \lambda_{pm} \\[2mm] \lambda_q = L_q i_q \\[2mm] \lambda_f = \dfrac{3}{2} M_{sf} i_f + L_f i_f + \lambda_{mf} \end{cases} \quad (2)$$

where λ_d represents the d-axis magnetic flux linkage of the stator, including the magnetic flux generated by the d-axis current, the magnetic flux generated by the permanent magnets, and the magnetic flux generated by the DC excitation winding; λ_q represents the q-axis magnetic flux of the stator; λ_f represents the magnetic flux linkage of the excitation winding turns; λ_{pm} represents the magnetic flux generated by the permanent magnets; λ_{mf} represents the magnetic flux passing through the excitation winding, which varies sinusoidally; L_d and L_q represent the d-axis and q-axis inductances of the stator windings, respectively; M_{sf} represents the mutual inductance between the excitation winding and the armature winding; L_f represents the self-inductance of excitation winding, i_d and i_q represent the d-axis and q-axis currents of the stator; and i_f represents the excitation current. u_d and u_q represent the d-axis and q-axis voltages of the stator, respectively; u_f represents the voltage of the excitation winding; ω_e represents the

rotational electrical angular velocity of the rotor; R_s represents the resistance of the stator phase winding and R_f represents the resistance of the excitation winding.

Based on the operation principle of the flux-switching PM (FSPM) motors [19], the electromagnetic output torque can be rewritten as

$$\begin{aligned} T_e &= T_{pm} + T_f + T_r \\ &= \frac{3}{2} P_r i_q \lambda_{pm} + \frac{3}{2} P_r i_q M_{sf} i_f + \frac{3}{2} P_r i_q \left(L_d - L_q\right) i_d \\ &= \frac{3}{2} P_r i_q \left[\lambda_{pm} + M_{sf} i_f + \left(L_d - L_q\right) i_d \right] \\ &= \frac{3}{2} P_r i_q \left[\lambda_{exc} + \left(L_d - L_q\right) i_d \right] \end{aligned} \quad (3)$$

where P represents the rotor poles number and $\lambda_{exc} = \lambda_{pm} + M_{sf} i_f$. The first term on the right-hand side of Equation (3), $1.5 p i_q \lambda_{pm}$, represents the PM torque, the second term, $1.5 p i_q M_{sf} i_f$, represents the DC excitation torque, and the third term, $1.5 p i_q i_d (L_d - L_q)$, represents the reluctance torque.

Losses in PM machines include copper losses, eddy current losses in PMs, and iron losses in both the stator and rotor. Eddy current losses in PMs are often overlooked because the primary air-gap magnetic field rotates with the rotor, leading to minimal temporal and spatial harmonics. Iron losses are categorized into hysteresis losses (P_h), eddy current losses (P_c), and excess losses (P_e). The material properties are crucial for calculating these losses. The core is made of steel 1010, which is widely available and of high quality. The B-H curve and loss curves for this material are illustrated in Fig. 6 (a) and 6 (b).

Iron losses are obtained as follows:

$$p_v = p_h + p_c + p_e = k_h f B_m^2 + k_c \left(f B_m\right)^2 + k_e \left(f B_m\right)^{1.5} \quad (4)$$

where k_h, k_c, and k_e represent the coefficients for hysteresis losses, eddy current losses, and excess losses, respectively. The peak value of magnetic flux density is denoted as B_m. These coefficients are determined using the least squares minimization method.

$$\begin{aligned} &min\left(error\left(k_h, k_c, k_e\right)\right) = \\ &\sum_{i=1}^{m} \sum_{j=1}^{n_i} \left[p_{vij} - \left(k_h f_i B_{mij}^2 + k_c \left(f_i B_{mij}\right)^2 + k_e \left(f_i B_{mij}\right)^{1.5} \right) \right]^2 \end{aligned} \quad (5)$$

where m is the number of loss curve branches, n_i is the number of points in the i-th curve, and $p_{vij} = f\left(f_i, B_{mij}\right)$ is a two-dimensional lookup table for losses at different frequencies. The efficiency map of the motor

featuring optimized structures is depicted in Fig. 6 (c). As illustrated, the optimized motor demonstrates a notably broad efficiency range exceeding 90%.
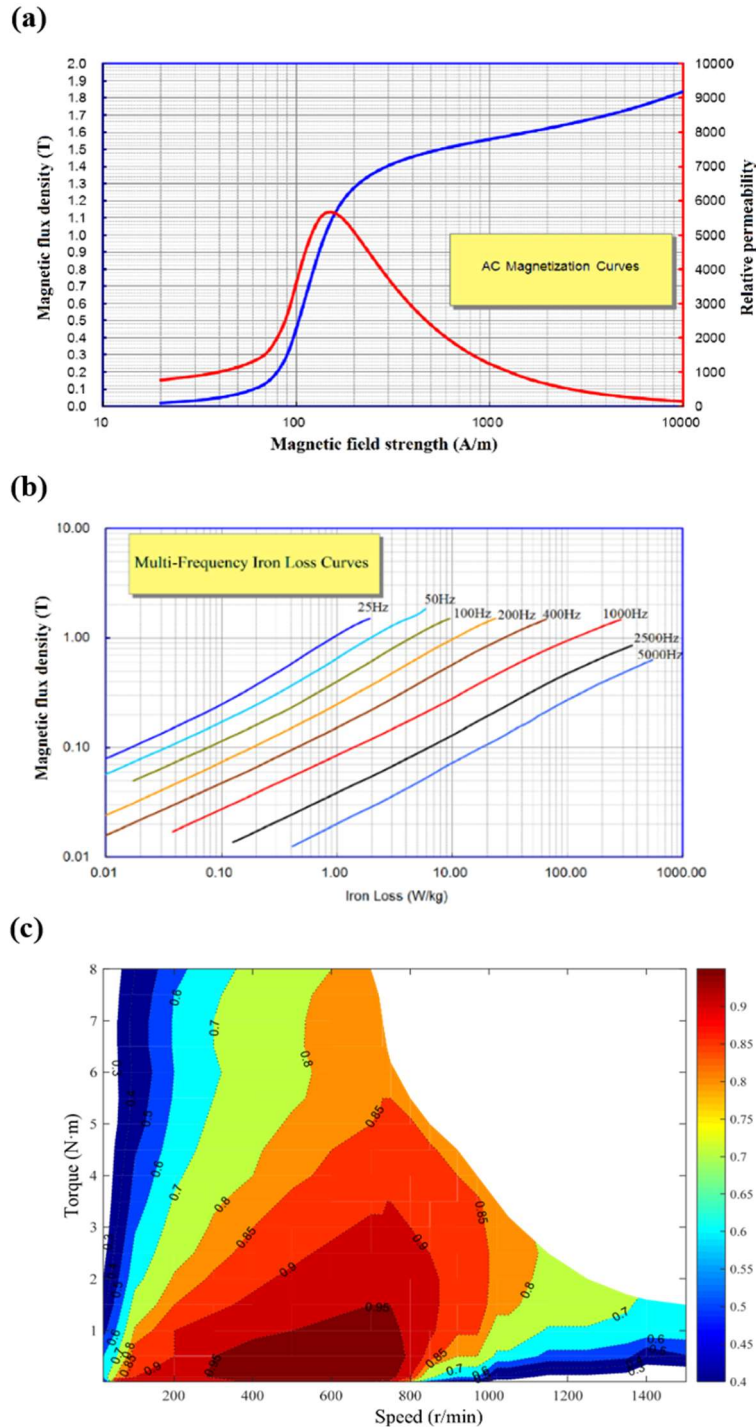
(a)

(b)

(c)

Fig. 6. (a) B-H curve of the core (b) Core loss curves at different frequencies (c) The efficiency map of optimized motor.

4 Voltage Difference-based Field-Weakening (VDFW) control Strategy

The DRHE-AFSPM motor and its associated drive system for EVs, as presented in this paper, exhibit two notable characteristics. First, in the low-speed operational range, field-enhancing control is applied to produce the high torque essential for vehicle startup and

climbing. Second, in the high-speed operational range, field-weakening control is implemented to extend the constant power operating range of the DRHE-AFSPM, thereby enabling the EV to function efficiently in high-speed cruising conditions.

Based on the characteristics of DRHE-AFSPM motor and the characteristics of EV drive systems, the operation of DRHE-AFSPM is divided into two regions, as shown in Fig. 7: Region (I) represents the low-speed region. The region II is the additional region due to the positive excitation current. The region III and IV are flux-weakening region.
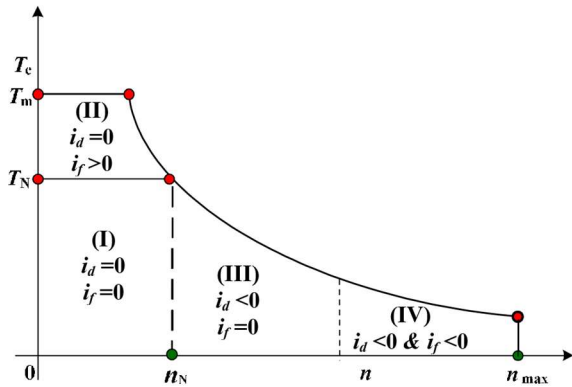

Fig. 7. Strategy of stage control for DRHE-AFSPM motor

Using the vector control method and the *d-q* coordinate system, the DRHE-AFSPM motor drive system is obtained, as shown in Fig. 8. The main functional modules include DRHE-AFSPM motor, voltage source inverter, Park transformation, 2s/2r transformation, space vector PWM (SVPWM), PWM, and reference current calculator, among others.

When the three-phase inverter output line voltage exceeds the DC bus voltage, the field weakening control method with different magnetic states further expands the motor speed control range and improves the motor's electromagnetic torque capability.

In the constant torque control region, the q-axis current reference is determined by the output of the speed regulator. In the constant power control region, the q-axis current reference is determined by the d-axis current and the maximum output current of the inverter, based on the current constraint condition.

The d-axis field weakening current is determined based on the difference between the inverter output line voltage and the DC bus voltage. This method is robust and does not depend on motor parameter variations. It can automatically activate the field weakening control mode even when the DC bus voltage drops unexpectedly, without the need for additional sensors, reducing the system cost. The value of the d-axis and q-axis reference currents, obtained as described above, determines the value of the output current i_f. In a scenario where the speed is less than the nominal speed and the load torque is also less than the rated torque, the reference current value becomes zero.
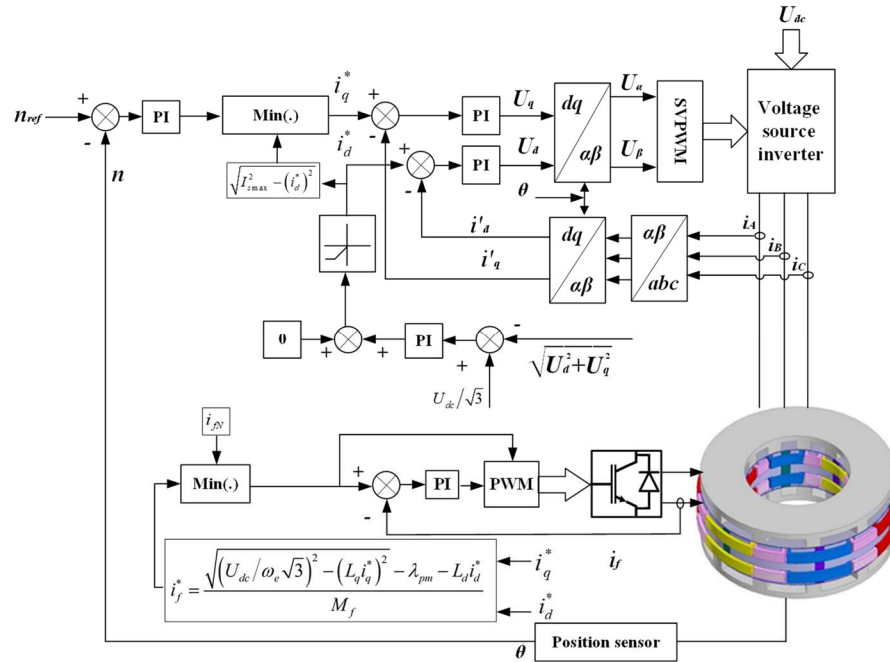

Fig. 8. Block diagram of control system for DRHE-AFSPM

Initially, using the voltage difference method, the reference current of d-axis is calculated. Subsequently,

based on the maximum allowable current, the reference current of q-axis is computed. Then, the reference current of q-axis is compared with the calculated q-axis current derived from the speed difference, and the minimum among them is considered as the reference q-axis current. The excitation field current is determined based on the q and d-axis reference currents, considering the voltage constraint circle, and compared with the nominal excitation current, selecting the minimum as the excitation current.

5 Simulation and Experiment

The parameters of the DRHE-AFSPM motor prototype used in this paper are shown in Table 1. In order to study the performance of DRHE-AFSPM motor and the effectiveness of the proposed algorithm, a DRHE-AFSPM motor simulation system is built based on Matlab/Simulink to analyze its static and dynamic characteristics. To further investigate the operational performance of DRHE-AFSPM motor, a driving control experiment is conducted on the prototype with the parameters given in Table 1 using the dSPACE1103 control platform. Fig. 9 shows the experimental platform for the drive system.

First, the field-weakening trajectory of DRHE-AFSPM is simulated based on the parameters given in Table 1.

Table 1. Parameters of DRHE-AFSPM motor

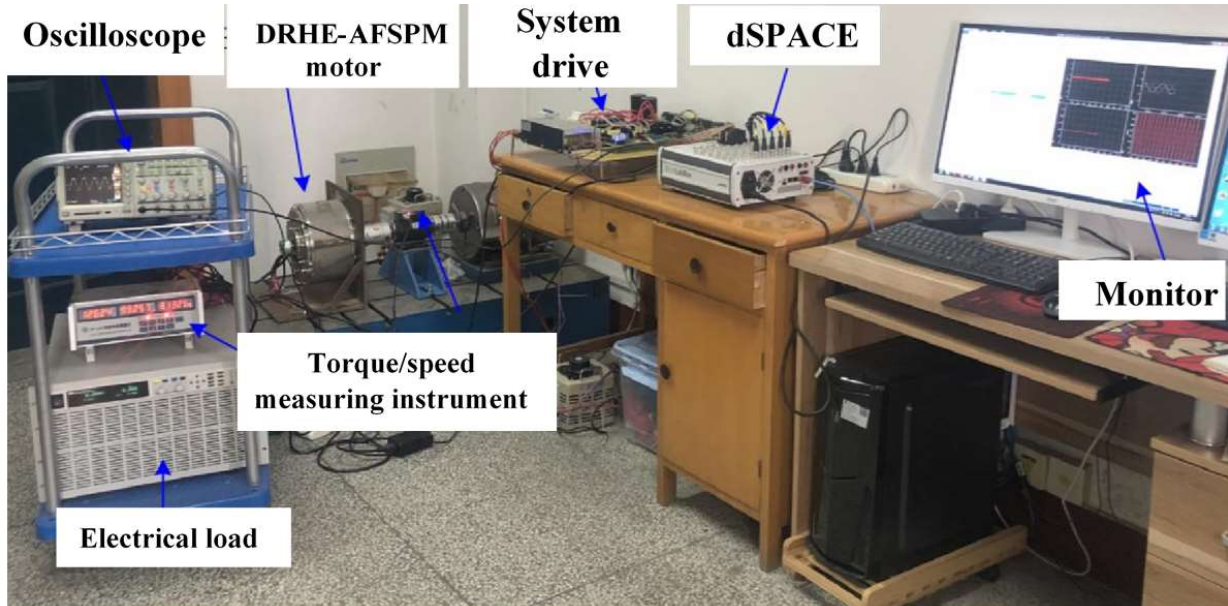| Parameters	value	Parameters	value
Bus voltage/V	200	PM flux linkage amplitude/Wb	0.05
Rated speed/(r/min)	750	Phase winding resistance/Ω	3.4
Rated torque (N·m)	12	Direct axis inductance/mH	10.4
Rated current/A	10	Quadrature axis inductance/mH	14.8
Number of rotor pole	11	stator teeth	12
Mutual inductance of armature and field winding/mH	18.1	Excitation current/A	6

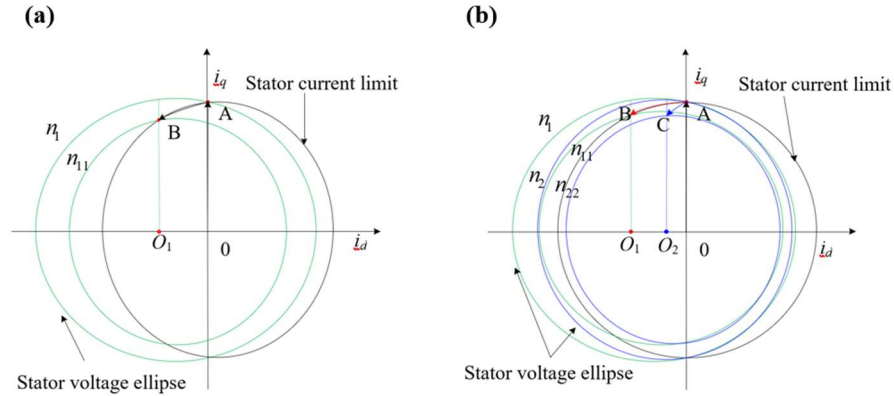**Fig. 9.** Experiment platform of control system for DRHE-AFSPM motor

Fig. 10. Voltage and current operating point trajectory of field weakening control combined with segmented magnetization state adjustment

Based on the above analysis, under a certain DC bus voltage, the current and voltage operating point trajectories of field weakening control combined with proposed method are shown in Fig.10. In the low-speed zone, as the speed given increases, the operating point changes from "0" to "A". When the given speed exceeds n_1, the field weakening current is used to further expand the speed to n_{11}, and the corresponding operating point changes from "A" to "B". The speed given further increases and exceeds n_{11}. As shown in Fig. 10 (b), the

magnetization state of the PM is changed by applying pulse current i_{f2}, so that the center of the stator voltage limit ellipse changes from "O_1" to "O_2". Therefore, in the speed range $(n_{11}, n_2]$, the PM flux linkage meets the speed and current tracking control requirements, and the corresponding operating point changes from "B" to "C". Similarly, the changes in the motor operating point when the rotational speed changes in other different speed ranges can be analyzed.
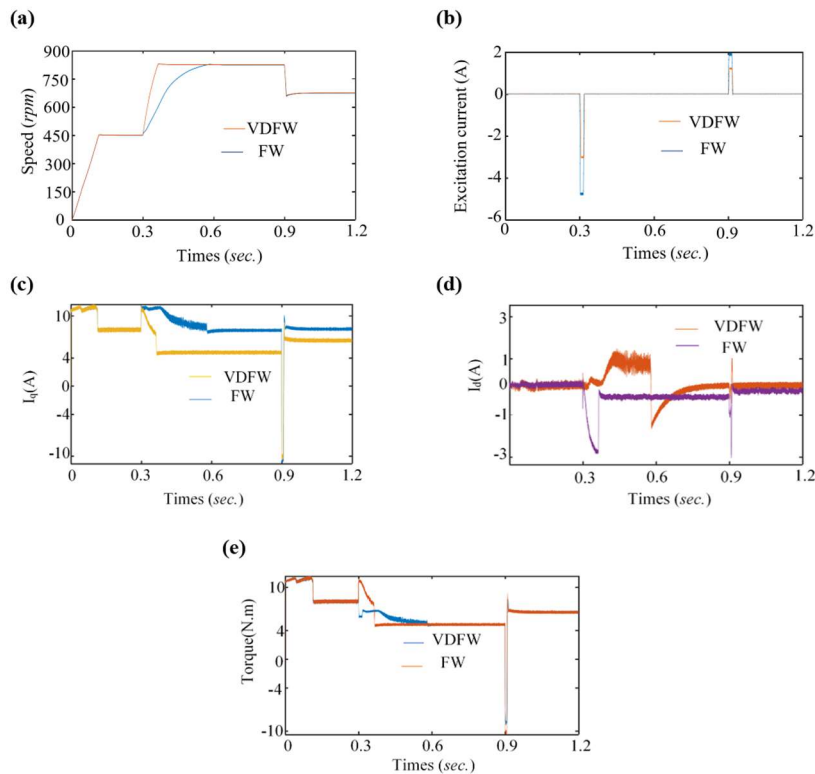

Fig. 11. Simulation comparison of VDFW and FW control. (a) Speed. (b) Excitation current. (c) i_q. (d) i_d. (e) Torque.

5.1 Simulation Results

The load torque settings corresponding to three different speed intervals of [0, 560], [560, 650] and [650, 780] r/min are 8, 7 and 4.8 N·m respectively. During the speed given mutation process, Fig. 11 shows the DRHE-AFSPM motor when the Voltage Difference-based Field-Weakening (VDFW) control Strategy and the Traditional Field-Weakening (FW) control Strategy Performance simulation comparison. The speed given is within the [0, 560] r/min speed range. Both VDFW and FW control method enable the motor to have the same torque, speed response and rated stator current. The speed reference is located in the [650, 780] r/min speed range. A negative pulse current with an amplitude of 4.8A needs to be applied to enable the optimal torque control combined to track the speed reference, while FW reduces the air gap magnetic density by applying -2.6As negative pulse current with an amplitude of 4.8A in the armature winding to achieve field weakening speed

expansion. Compared with traditional field weakening control, the optimal torque control combined with magnetization state adjustment reduces the PM flux linkage, making the motor have a slower speed response. The speed given is within the [750, 865] r/min speed range, and the impact of the two control methods on motor performance can be analyzed similarly.

The dynamic simulation of the DRHE-AFSPM motor at high speed (1400 rpm), shown in Fig. 12, indicates that the motor enters the field-weakening operation region at 780 rpm. This result confirms the proposed strategy for determining field-weakening moments based on the differences between bus voltage and back EMF. This approach optimizes inverter output voltage and extends the motor's speed range. After entering the field-weakening region, the motor first reduces the magnetic field using an excitation current i_f of approximately -4.5 A, followed by negative i_d for further weakening until reaching the target speed of 1400 rpm.
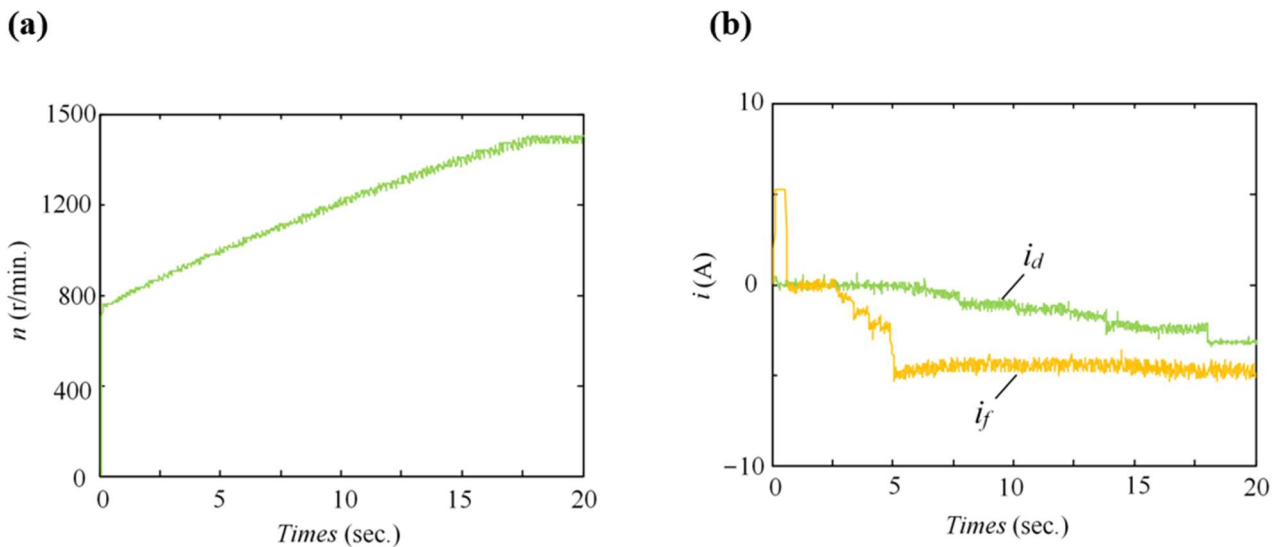

Fig. 12. Simulation results of dynamic characteristics for DRHE-AFSPM in high speed operating region (a) Speed (b) i_d and i_f

5.2 Experiment results

When a load torque of 10 N·m is applied and there is a sudden change in the speed command, the performance of the DRHE-AFSPM with the VDFW control strategy is compared to that of the FW control, as depicted in Fig. 13. During the startup from standstill to 400 rpm, the speed command rises to 800 rpm. In Fig. 13, it is observed that the PM flux linkage is approximately 0.05 Wb and no i_f is applied .However, the motor cannot track the speed given under the FW control. At the same time, the direct-axis current of the VDFW control combined

with magnetization state adjustment changes with the rotation speed, while the direct-axis current of the FW control is limited to the maximum field-weakening current. The system employing the proposed control exhibits quicker speed response and higher torque capability compared to the FW control. However, with the FW control, in order to track the speed command, a negative pulse is required to weaken the magnetic saturation. Additionally, under constant load torque, higher PM flux linkage results in lower armature current.
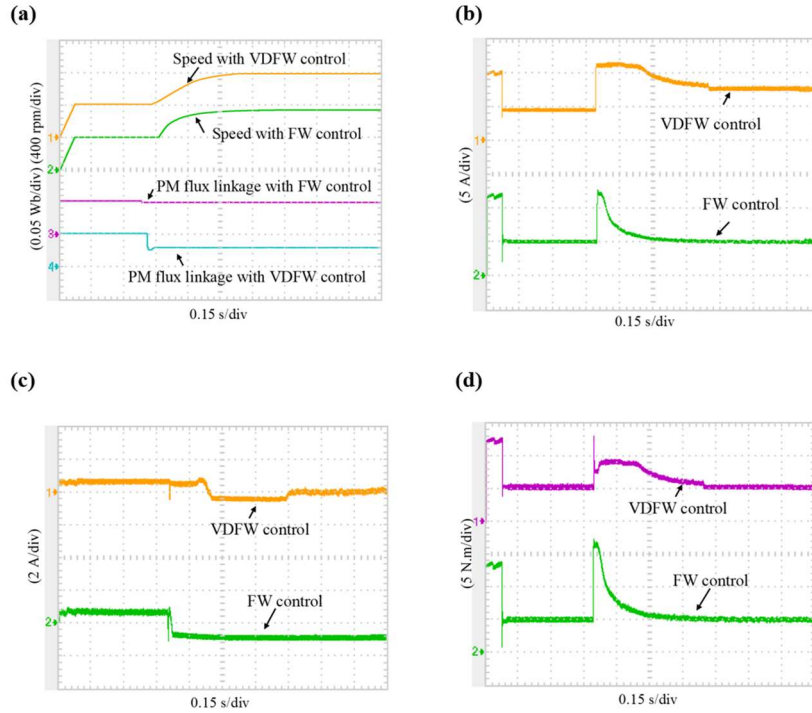
Fig. 13. Performance comparison between VDFW control and traditional FW control. (a) speed and PM flux linkage. (b) i_q. (c) i_d. (d) torque.
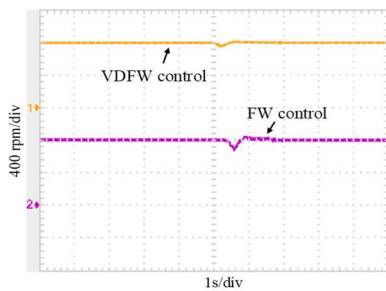

Fig. 14. Speed waveform of sudden load

The speed experiment graph shown in Fig. 14 illustrates the speed test results of the motor when a sudden load is applied during stable operation at 800 rpm. From the graph, it can be observed that the speed drop with a FW controller is approximately 50 rpm, while with the VDFW controller, the speed drop is only 25 rpm, and it returns to a stable state faster. The experiment indicates that the VDFW algorithm enhances the system's robustness.

The performance of the DRHE-AFSPM motor in the high-speed range is depicted in Fig.15. The motor was started with no load at a speed of 1500 rpm. In Fig. 15, it is evident that as the speed approaches 800 rpm, the DRHE-AFSPM motor enters the field-weakening operation region. This demonstrates the effectiveness of the field-weakening moment determination strategy proposed. This approach allows for the maximum

utilization of the inverter's output voltage and expands the motor's speed range. Moreover, Fig. 15 illustrates the motor's behavior after entering the field-weakening region. The DRHE-AFSPM motor initially weakens the magnetic field by adjusting the excitation current i_f. As the excitation current if reaches approximately -5 A, negative i_d is employed for further field weakening until the motor reaches the desired speed of 1500 rpm. These experimental findings are consistent with the theoretical analysis and simulation results.
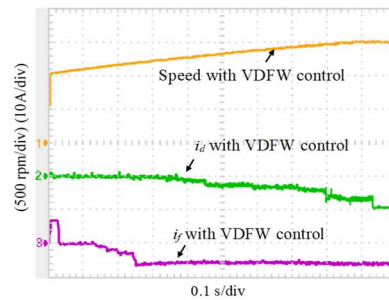

Fig. 15. DRHE-AFSPM in high speed operating region

6 Conclusion

This study presents an innovative approach to flux machine control by integrating a unique flux-weakening control strategy in the hybrid PM axial field flux-switching machine. This method not only extends the operational speed range of the machine but also

enhances torque, thereby making a significant contribution to the advancement of flux machine control technology. The analysis begins with a thorough examination of the machine's topology, the magnetic field regulation mechanism, and the inductance characteristics of the DRHE-AFSPM motor. Following this, the mathematical model of the DRHE-AFSPM is derived using the d-q rotating coordinate system, providing a robust framework for further analysis. A control model for the drive system of the DRHE-AFSPM motor is then established based on a partitioned control strategy. In the low-speed operational range, a control approach is proposed that maintains id=0 while exclusively utilizing excitation current for field weakening. For high-speed operations, a field weakening control strategy based on voltage difference determination is introduced, facilitating effective field weakening control for the DRHE-AFSPM motor. The control strategy proposed in this study, which maintains id=0 and relies solely on excitation current for field weakening, significantly enhances load capacity and optimally utilizes the motor's output torque. Furthermore, the field weakening control strategy based on voltage difference determination maximizes the inverter's output voltage utilization, broadens the motor's operational speed range, and increases load capacity at equivalent speeds. This comprehensive approach not only improves the performance of the DRHE-AFSPM motor but also sets a new standard for flux machine control methodologies.

Conflict of Interest

The authors declare no conflict of interest.

Funding

References

[1] Li, J., K. Wang, and C. Liu. "Improvement of integrated-induction-based hybrid excitation brushless DC generator by employing novel consequent-pole rotor." IEEE Transactions on Industrial Electronics 69, no. 12 (2022): 12042-12054.

[2] Mörée, Gustav, and Mats Leijon. "Overview of hybrid excitation in electrical machines." Energies 15, no. 19 (2022): 7254.

[3] Geng, Huihui, Xueyi Zhang, Shilong Yan, Lanian Tong, Qingzhi Ma, Mingjun Xu, Yufeng Zhang, and Yutong Han. "Magnetic field analysis and performance optimization of hybrid excitation generators for vehicles." Sustainable Energy Technologies and Assessments 52 (2022): 102200.

[4] Fan, Ying, Yutong Lei, and Xu Wang. "An Improved Robust Deadbeat Predictive Current Control for the Consequent-pole Hybrid Excitation Motor." IEEE Transactions on Energy Conversion (2023).

[5] Dong, Tenghui, Yunfei Gao, and Taketsune Nakamura. "High Fault-Tolerance Dual-Rotor Synchronous Machine With Hybrid Excitation Field Generated by Halbach Permanent Magnets and High Temperature Superconducting Magnets." IEEE Transactions on Applied Superconductivity 33, no. 5 (2023): 1-5.

[6] Al-Adsani, A.S., Beik, O. (2022). Hybrid Electric Machine Concept. In: Multiphase Hybrid Electric Machines. Springer, Cham. https://doi.org/10.1007/978-3-030-80435-0_2

[7] Limsuwan, Natee, Takashi Kato, Kan Akatsu, and Robert D. Lorenz. "Design and evaluation of a variable-flux flux-intensifying interior permanent-magnet machine." IEEE Transactions on Industry Applications 50, no. 2 (2013): 1015-1024.

[8] Yu, Chen-Yen, Takashi Fukushige, Natee Limsuwan, Takashi Kato, David Diaz Reigosa, and Robert D. Lorenz. "Variable-flux machine torque estimation and pulsating torque mitigation during magnetization state manipulation." IEEE Transactions on Industry Applications 50, no. 5 (2014): 3414-3422.

[9] Fukushige, Takashi, Natee Limsuwan, Takashi Kato, Kan Akatsu, and Robert D. Lorenz. "Efficiency contours and loss minimization over a driving cycle of a variable flux-intensifying machine." IEEE Transactions on Industry Applications 51, no. 4 (2015): 2984-2989.

[10] Yu, Chen-Yen, Takashi Fukushige, Apoorva Athavale, Brent Gagas, Kan Akatsu, David Reigosa, and Robert D. Lorenz. "Zero/low speed magnet magnetization state estimation using high frequency injection for a fractional slot variable flux-intensifying interior permanent magnet synchronous machine." In 2014 IEEE Energy Conversion Congress and Exposition (ECCE), pp. 2495-2502. IEEE, 2014.

[11] Chen, Junhua, Jian Li, and Ronghai Qu. "Maximum-torque-per-ampere and magnetization-state control of a variable-flux permanent magnet machine." IEEE Transactions on Industrial Electronics 65, no. 2 (2017): 1158-1169.

[12] Yu, Chuang, and K. T. Chau. "Dual-mode operation of DC-excited memory motors under flux regulation." IEEE Transactions on Industry Applications 47, no. 5 (2011): 2031-2041.

[13] Zhao, Jilong, Mingyao Lin, Long Jin, and Wei Zhang. "Vector control study of axial field flux-switching permanent magnet machine." In 2014 17th International Conference on Electrical Machines and Systems (ICEMS), pp. 1091-1095. IEEE, 2014.

[14] Jung, Sung-Yoon, Chunting Chris Mi, and Kwanghee Nam. "Torque control of IPMSM in the field-weakening region with improved DC-link voltage utilization." IEEE Transactions on Industrial Electronics 62, no. 6 (2014): 3380-3387.

[15] Aydin, Metin, Surong Huang, and Thomas A. Lipo. "Design, analysis, and control of a hybrid field-controlled axial-flux permanent-magnet motor." IEEE Transactions on industrial electronics 57, no. 1 (2009): 78-87.

[16] Deng, Tao, Zhenhua Su, Junying Li, Peng Tang, Xing Chen, and Ping Liu. "Advanced angle field weakening control strategy of permanent magnet synchronous motor." IEEE Transactions on Vehicular Technology 68, no. 4 (2019): 3424-3435.

[17] Fard, J. Rahmani. "A Novel High-Performance Field-Weakening Control for Axial Flux-Switching Permanent-Magnet Motor." Iranian Journal of Electrical & Electronic Engineering 16, no. 1 (2020).

[18] Zhao, Jilong, Xiaowei Quan, Xiangdong Sun, Mingyao Lin, and Shuangxia Niu. "Influence of rotor-pole number on electromagnetic performance of novel double-rotor hybrid excited axial switched-flux permanent-magnet machines for EV/HEV applications." IEEE Transactions on Magnetics 56, no. 3 (2020): 1-6.

[19] Ding, Wen, and Shuai Li. "Maximum ratio of torque to copper loss control for hybrid excited flux-switching machine in whole speed range." IEEE Transactions on Industrial Electronics 66, no. 2 (2018): 932-943.

research interests include the modeling and design of electrical machines, drive systems, control and optimization of power systems, performance analysis and dynamics of electrical machines, and the application of the Finite Element Method (FEM).

B. Rezaeealam received the B.S. degree from Isfahan University of Technology in 1997, the M.S. and Ph.D. degrees from University of Tehran in 2000 and 2005, respectively, all in electrical engineering. He is currently an associate professor in the department of electrical engineering, Lorestan University, Iran. His research interests include modeling and design using FEM, electrical machines and drives.

M. Kamali received his Bachelor's degree in Electrical Engineering from Islamic Azad University, Khorramabad Branch, in 2014, and his Master's degree in Electrical Engineering from Lorestan University in 2021. He is currently pursuing a Ph.D. in Electrical Engineering at Lorestan University. His

F. Rezaee-Alam received the B.S. degree from Shahid Chamran University of Ahwaz in 2007, the M.S. and Ph.D. degrees from Khajeh Nasir University of Technology in 2010 and 2015, respectively, all in electrical engineering. He is currently an associate professor in the department of electrical engineering, Lorestan University, Iran. His research interests include design and modeling of electric machines.